smaller. For all but nearly stationary shocks, any such oscillations are rapidly damped downstream from the shock. The effective shock width is never more than two mesh lengths, and for rapidly moving shocks it is one mesh length. Experimentation with different values of the parameters is not recommended, as these choices have been made on the basis of considerable experience.

ACKNOWLEDGMENTS

This work was performed under the auspices of the Director, Office of Energy Research, Office of Basic Energy Sciences, Engineering, Mathematical, and Geosciences Division of the U.S. Department of Energy at the Lawrence Berkeley Laboratory under Contract DE-AC03-76SF00098, and at the Lawrence Livermore National Laboratory under Contract W-7405-ENG-48.

REFERENCES

1. P. R. WOODWARD AND P. COLELLA, *Lecture Notes in Physics* **141** (1981), 434.
2. P. R. WOODWARD AND P. COLELLA, *J. Comput. Phys.* **54** (1984), 115–173.
3. S. K. GODUNOV, *Mat. Sb.* **47** (1959), 271.
4. S. K. GODUNOV, A. V. ZABRODIN, AND G. P. PROKOPOV, *U.S.S.R. Computational Math. and Math. Phys.* **1** (1961), 1187.
5. B. VAN LEER, *J. Comput. Phys.* **32** (1979), 101.
6. B. VAN LEER AND P. R. WOODWARD, Proceedings TICOM Conference, Austin, Texas, 1979.
7. P. COLELLA, A direct Eulerian MUSCL scheme for gas dynamics, *SIAM J. Sci. Statist. Comput.*, in press.
8. B. VAN LEER, *J. Comput. Phys.* **23** (1977), 276.
9. B. VAN LEER, private communication.
10. R. COURANT AND K. O. FRIEDRICHS, "Supersonic Flow and Shock Waves," Wiley–Interscience, New York, 1948.
11. A. LAPIDUS, *J. Comput. Phys.* **2** (1967), 154.
12. P. COLELLA AND H. M. GLAZ, Efficient solution algorithms for the Riemann problem for real gases, in preparation.

Printed by the St. Catherine Press Ltd., Tempelhof 41, Bruges, Belgium

Reprinted from JOURNAL OF COMPUTATIONAL PHYSICS
All Rights Reserved by Academic Press, New York and London

Vol. 54, No. 1, April 1984
Printed in Belgium

The Piecewise Parabolic Method (PPM) for Gas-Dynamical Simulations

PHILLIP COLELLA

Lawrence Berkeley Laboratory, University of California, Berkeley, California, 94720

AND

PAUL R. WOODWARD

Lawrence Livermore National Laboratory, University of California, Livermore, California 94550

Received August 3, 1982; revised August 25, 1983

We present the piecewise parabolic method, a higher-order extension of Godunov's method. There are several new features of this method which distinguish it from other higher-order Godunov-type methods. We use a higher-order spatial interpolation than previously used, which allows for a steeper representation of discontinuities, particularly contact discontinuities. We introduce a simpler and more robust algorithm for calculating the nonlinear wave interactions used to compute fluxes. Finally, we recognize the need for additional dissipation in any higher-order Godunov method of this type, and introduce it in such a way so as not to degrade the quality of the results.

INTRODUCTION

In [1] and [2], we presented an extensive comparison of various numerical methods for shock hydrodynamics. The most accurate of the methods tested was the piecewise parabolic method (PPM), developed by the authors. In this paper, we present a detailed description of the PPM scheme for gas dynamics in Lagrangian and Eulerian coordinates.

The PPM scheme is a higher-order extension of Godunov's method [3, 4] of a type first introduced by van Leer in his MUSCL algorithm [5, 6]. A more recent version of the MUSCL algorithm which is better suited for calculating strong shocks was presented in [7]. The PPM scheme represents a substantial advance over both these versions of MUSCL in several respects. First, the introduction of parabolae as the

[1] Work performed under the auspices of the Director, Office of Energy Research, Office of Basic Energy Sciences, Engineering, Mathematical, and Geosciences Division of the U.S. Department of Energy at the Lawrence Berkeley Laboratory under Contract DE-ACO3-76SF00098, and at the Lawrence Livermore National Laboratory under Contract W-7405-ENG-48.

0021-9991/84 $3.00
Copyright © 1984 by Academic Press, Inc.
All rights of reproduction in any form reserved.

basic interpolation functions in a zone allows for a more accurate representation of smooth spatial gradients, as well as a steeper representation of captured discontinuities, particularly contact discontinuities. Second, the representation of the nonlinear wave interactions used to compute fluxes is substantially simpler than that used in [7], giving rise to a less complicated and more robust algorithm. Finally, we have determined that additional dissipation beyond that given by monotonicity algorithms of the type discussed in [5] is required to obtain acceptably accurate results from any higher-order Godunov method of this type. We have made a careful study of the kind and amount of dissipation which is needed, and have found ways of introducing it which do not significantly degrade the quality of the computed solution.

This paper is divided into five sections. The first section describes the PPM scheme for a scalar advection equation, and establishes the interpolation formulae and techniques required for solving the gas dynamics equations. The second and third sections describe, respectively, the basic PPM scheme for gas dynamics in Lagrangian coordinates, and a single-step formulation of the scheme for gas dynamics in Eulerian coordinates. The Eulerian schemes described here are all for one space variable; the extension to more than one dimension is done using operator splitting. The fourth section discusses, in general terms, the kinds of dissipation required in these schemes; the final section is for discussion and conclusions. There is also an Appendix, which gives a detailed description of the dissipation algorithms used in the PPM calculations presented in [2].

1. The PPM Advection Scheme

In this section, we describe the PPM scheme for solving a linear advection equation

$$\frac{\partial a}{\partial t} + u\frac{\partial a}{\partial \xi} = 0 \qquad a(\xi, 0) = a_0(\xi). \tag{1.1}$$

Particular care has been taken to provide details of the algorithm for the case of a general unequally spaced mesh. One widely used formulation of Eulerian hydrodynamics algorithms is that of performing a hydrodynamics calculation for one time step using a Lagrangian method, and mapping the results onto the fixed Eulerian grid. In such an algorithm, the mapping step is essentially one step of a conservative advection algorithm. Since the mesh moves by varying amounts in the Lagrangian step, the mesh for which the mapping is performed is unequally spaced, even if the underlying Eulerian mesh is equally spaced. Thus, the algorithm described below, in the case of unequally spaced zones, has been extensively tested in the calculations in [2] performed using the version of the PPM hydrodynamics algorithm formulated as a Lagrangian step, followed by a remap.

Copyright © 1984 by Academic Press, Inc.
All rights reserved.

Let $\xi_{j+1/2}$ be the boundary between the jth and the $j+1$st zones on the computational grid, and assume that we know a_j^n, the average value of the solution a between $\xi_{j+1/2}$ and $\xi_{j-1/2}$ at time t^n:

$$a_j^n = \frac{1}{\Delta\xi_j}\int_{\xi_{j-1/2}}^{\xi_{j+1/2}} a(\xi, t^n)\, d\xi \qquad \Delta\xi_j = \xi_{j+1/2} - \xi_{j-1/2}. \tag{1.2}$$

We want to calculate a_j^{n+1}, the average value of the solution at time $t^{n+1} = t^n + \Delta t$, where Δt satisfies the stability condition $u\Delta t \leqslant \min_j \Delta\xi_j$. The advection scheme we will describe here is constructed following the approach to advection taken by van Leer in [8]. First, we construct a piecewise polynomial interpolation function $a(\xi)$ satisfying the condition

$$a_j^n = \frac{1}{\Delta\xi_j}\int_{\xi_{j-1/2}}^{\xi_{j+1/2}} a(\xi)\, d\xi$$

and constrained in such a way so that no new extrema appear in the interpolation function which do not already appear in the a_j^n's (Fig. 1). We can calculate explicitly the exact solution to Eq. (1.1) with inital values $a(\xi)$, i.e., $a(\xi, t^n + \Delta t) = a(\xi - u\Delta t)$ (Fig. 2). We integrate this solution over each zone to obtain a_j^{n+1}:

$$a_j^{n+1} = \frac{1}{\Delta\xi_j}\int_{\xi_{j-1/2}}^{\xi_{j+1/2}} a(\xi - u\Delta t)\, d\xi. \tag{1.3}$$

The scheme is uniquely determined by our choice of interpolation polynomial. The PPM scheme uses an interpolation which is piecewise continuous, with a given by a parabolic profile in each zone:

$$a(\xi) = a_{L,j} + x(\Delta a_j + a_{6,j}(1-x)) \qquad x = \frac{\xi - \xi_{j-1/2}}{\Delta\xi_j}, \qquad \xi_{j-1/2} \leqslant \xi \leqslant \xi_{j+1/2}. \tag{1.4}$$

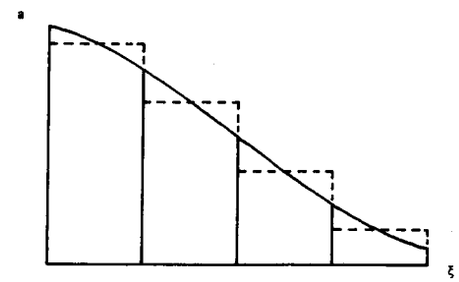

FIG. 1. The interpolation step of the PPM advection scheme. The initial data are given as values of the variable a averaged over the four zones shown. These averaged values are represented by dashed lines. From this data values of the variable a are interpolated at zone edges, using cubic curves which have the prescribed average values in the four zones nearest the edge. The interpolation parabolae within the zones, which are shown as solid lines, connect these edge values and give back the initial data when averaged over the zones.

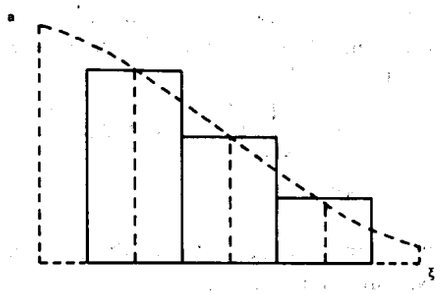

FIG. 2. The integration step of the PPM advection scheme. New averages of the variable a within the zones are obtained by integrating over the interpolated initial distribution shifted to the right by $u\Delta t$. This shifted distribution is shown by the dashed lines, and the new zone averages are shown by the solid lines. The scheme is third-order accurate in general; in the limit of very small time steps, for equally spaced zones, it is fourth-order accurate.

It is a straightforward bit of algebra to verify that the coefficients of this polynomial can be derived from a_j^n, and the values $\lim_{\xi\downarrow\xi_{j-1/2}} a(\xi) = a_{L,j}$, $\lim_{\xi\uparrow\xi_{j+1/2}} a(\xi) = a_{R,j}$:

$$\Delta a_j = a_{R,j} - a_{L,j}, \qquad a_{6,j} = 6(a_j^n - \tfrac{1}{2}(a_{L,j} + a_{R,j})). \tag{1.5}$$

We calculate $a_{L,j}$ and $a_{R,j}$ by first using an interpolation scheme to calculate $a_{j+1/2}$, an approximation to the value of a at $\xi_{j+1/2}$, subject to the constraint that $a_{j+1/2}$ does not fall out of the range of values given by a_j and a_{j+1}. In smooth parts of the solution, away from extrema, $a_{L,j+1} = a_{R,j} = a_{j+1/2}$, so that the interpolation function $a(\xi)$ is continuous at $\xi_{j+1/2}$. The values $a_{L,j}$ and $a_{R,j}$ are further modified so that $a(\xi)$ is a monotone function on each interval $(\xi_{j-1/2}, \xi_{j+1/2})$. It is this step that introduces the discontinuities at zone edges.

Given the averages a_j^n of a in nearby zones, we want to interpolate a value $a_{j+1/2}$. Equivalently, we know the values of the indefinite integral of a, $A(\xi) = \int^{\xi} a(\xi', t^n)\, d\xi'$, at zone edges:

$$A(\xi_{j+1/2}) = A_{j+1/2} = \sum_{k\leq j} a_k^n \Delta\xi_k.$$

To calculate $a_{j+1/2}$, we interpolate the quartic polynomial through the points $(A_{j+k+1/2}, \xi_{j+k+1/2})$, $k = 0, \pm 1, \pm 2$, and differentiate it to obtain $a_{j+1/2} = dA/d\xi|_{\xi_{j+1/2}}$. The formula for $a_{j+1/2}$ so obtained, in terms of the $\xi_{j+1/2}$'s and the a_j^n's, is given by

$$\begin{aligned} a_{j+1/2} = a_j^n &+ \frac{\Delta\xi_j}{\Delta\xi_j + \Delta\xi_{j+1}}(a_{j+1}^n - a_j^n) + \frac{1}{\sum_{k=-1}^{2} \Delta\xi_{j+k}} \\ &\times \left\{ \frac{2\Delta\xi_{j+1}\Delta\xi_j}{\Delta\xi_j + \Delta\xi_{j+1}} \left[\frac{\Delta\xi_{j-1} + \Delta\xi_j}{2\Delta\xi_j + \Delta\xi_{j+1}} - \frac{\Delta\xi_{j+2} + \Delta\xi_{j+1}}{2\Delta\xi_{j+1} + \Delta\xi_j} \right] (a_{j+1}^n - a_j^n) \right. \\ &\left. - \Delta\xi_j \frac{\Delta\xi_{j-1} + \Delta\xi_j}{2\Delta\xi_j + \Delta\xi_{j+1}} \delta a_{j+1} + \Delta\xi_{j+1} \frac{\Delta\xi_{j+1} + \Delta\xi_{j+2}}{\Delta\xi_j + 2\Delta\xi_{j+1}} \delta a_j \right\}. \end{aligned} \tag{1.6}$$

Here δa_j is the average slope in the jth zone of the parabola with zone averages a_{j-1}^n and a_j^n, a_{j+1}^n, and is given by

$$\delta a_j = \frac{\Delta\xi_j}{\Delta\xi_{j-1} + \Delta\xi_j + \Delta\xi_{j+1}} \left[\frac{2\Delta\xi_{j-1} + \Delta\xi_j}{\Delta\xi_{j+1} + \Delta\xi_j}(a_{j+1}^n - a_j^n) + \frac{\Delta\xi_j + 2\Delta\xi_{j+1}}{\Delta\xi_{j-1} + \Delta\xi_j}(a_j^n - a_{j-1}^n) \right]. \tag{1.7}$$

In the calculations performed here and in [2], we have replaced δa_j in the above expression by $\delta_m a_j$, defined to be

$$\begin{aligned} \delta_m a_j &= \min(|\delta a_j|, 2|a_j^n - a_{j-1}^n|, 2|a_j^n - a_{j-1}^n|)\,\mathrm{sgn}(\delta a_j) \\ &\quad \text{if } (a_{j+1}^n - a_j^n)(a_j^n - a_{j-1}^n) > 0 \\ &= 0 \text{ otherwise.} \end{aligned} \tag{1.8}$$

This modification leads to a somewhat steeper representation of discontinuities in the solution. It also guarantees that $a_{j+1/2}$ lies in the range of values defined by a_j^n and a_{j+1}^n.

This calculation yields a value for $a_{j+1/2}$ which is third-order accurate for variable mesh spacing, even where the mesh spacing changes discontinuously. If the zones are equally spaced, and if $\delta a_j = \delta_m a_j$, then the values obtained are given by the following simple formula:

$$a_{j+1/2} = \frac{7}{12}(a_j^n + a_{j+1}^n) - \frac{1}{12}(a_{j+2}^n + a_{j-1}^n). \tag{1.9}$$

In regions where the solution is smooth, and in the limit of vanishing time step, the PPM advection scheme for equally spaced zones is fourth-order accurate.

The value $a_{j+1/2}$ will be assigned to $a_{L,j}$ and $a_{R,j-1}$ for most values of j. There are some cases, however, where this would lead to an interpolation function which takes on values not between $a_{L,j}$ and $a_{R,j}$. In such cases, we reset one or both of these values. There are two cases. First, if a_j^n is a local maximum or minimum, then the interpolation function is set to be a constant. The second case is where a_j^n is between $a_{R,j}$ and $a_{L,j}$, but sufficiently close to one of the values so that the interpolated parabola takes on a value which is not between $a_{R,j}$ and $a_{L,j}$. The condition on the coefficients of the interpolating parabola such that it does not overshoot is that $|\Delta a_j| \geqslant |a_{6,j}|$. When this condition fails to hold, either $a_{L,j}$ or $a_{R,j}$ is reset, so that the interpolation parabola is monotone, and so that its derivative at the opposite edge of the zone from the one where the value is being reset is zero. The expressions for $a_{L,j}$ and $a_{R,j}$ are as follows:

$$
\begin{aligned}
&a_{L,j} \to a_j^n, \quad a_{R,j} \to a_j^n \quad \text{if} \quad (a_{R,j} - a_j^n)(a_j^n - a_{L,j}) \leqslant 0 \\
&a_{L,j} \to 3a_j^n - 2a_{R,j} \quad \text{if} \quad (a_{R,j} - a_{L,j})\left(a_j^n - \frac{1}{2}(a_{L,j} + a_{R,j})\right) > \frac{(a_{R,j} - a_{L,j})^2}{6} \\
&a_{R,j} \to 3a_j^n - 2a_{L,j} \quad \text{if} \quad -\frac{(a_{R,j} - a_{L,j})^2}{6} > (a_{R,j} - a_{L,j})\left(a_j^n - \frac{1}{2}(a_{R,j} + a_{L,j})\right).
\end{aligned}
\tag{1.10}
$$

This completes our description of the calculation of $a_{L,j}$ and $a_{R,j}$. Once we have these values, it is easy to write down an explicit expression for a_j^{n+1}. We define averages of the interpolation functions

$$
\begin{aligned}
f^a_{j+1/2,L}(y) &= \frac{1}{y}\int_{\xi_{j+1/2}-y}^{\xi_{j+1/2}} a(\xi)\, d\xi \\
f^a_{j+1/2,R}(y) &= \frac{1}{y}\int_{\xi_{j+1/2}}^{\xi_{j+1/2}+y} a(\xi)\, d\xi
\end{aligned}
\tag{1.11}
$$

where y is assumed to be positive. Then it is easy to check that

$$
\begin{aligned}
f^a_{j+1/2,L}(y) &= a_{R,j} - \frac{x}{2}\left(\Delta a_j - \left(1 - \frac{2}{3}x\right) a_{6,j}\right), \qquad \text{for} \quad x = \frac{y}{\Delta\xi_j} \\
f^a_{j+1/2,R}(y) &= a_{L,j+1} + \frac{x}{2}\left(\Delta a_{j+1} + \left(1 - \frac{2}{3}x\right) a_{6,j+1}\right), \qquad \text{for} \quad x = \frac{y}{\Delta\xi_{j+1}}.
\end{aligned}
\tag{1.12}
$$

Then we can express the calculation of a_j^{n+1} in explicit conservation form:

$$
a_j^{n+1} = a_j^n + u\frac{\Delta t}{\Delta\xi_j}(\bar{a}_{j-1/2} - \bar{a}_{j+1/2}), \tag{1.13}
$$

where

$$
\begin{aligned}
\bar{a}_{j+1/2} &= f^a_{j+1/2,L}(u\Delta t), \qquad \text{if} \quad u \geqslant 0 \\
&= f^a_{j+1/2,R}(-u\Delta t), \qquad \text{if} \quad u \leqslant 0.
\end{aligned}
$$

We can modify the interpolation procedure slightly so that, in the neighborhood of a discontinuity, it produces a narrower profile than the scheme described above. If the jth zone is determined to be inside a discontinuity, then, instead of setting $a_{R,j}$ equal to $a_{j+1/2}$ using Eq. (1.6), we use the piecewise linear distribution given by $\delta_m a_{j+1}$ in Eq. (1.8). Similarly, to compute $a_{L,j}$, we use $\delta_m a_{j-1}$:

$$
a_{L,j} \to a^d_{L,j} = a_{j-1} + \tfrac{1}{2}\delta_m a_{j-1}, \qquad a_{R,j} \to a^d_{R,j} = a_{j+1} - \tfrac{1}{2}\delta_m a_{j+1}. \tag{1.14}
$$

This substitution should be performed just prior to applying the monotonicity algorithm (1.10).

In Fig. 3, we show an example of the effect of such a substitution, which we shall refer to as discontinuity detection. The dotted line represents the interpolation function in the jth zone without detection, obtained by using the difference formula (1.6) in calculating $a_{L,j}$ and $a_{R,j}$. The solid line is the interpolated distribution obtained by using for $a_{L,j}$ and $a_{R,j}$ values obtained from the piecewise linear distributions in neighboring zones determined by Eqs. (1.7) and (1.8). These linear distributions are shown here as dashed lines. Because of the monotonicity constraint (1.8) which is imposed on these distributions, the dashed lines are nearly horizontal, so that $a_{L,j}$ and $a_{R,j}$ are nearly equal to the left and right limiting values for the full discontinuity. Consequently, the interpolated profile is steeper, and the advected discontinuity remains sharper. Another feature of this detection algorithm is that if it detects a discontinuity in a region where in fact the solution is continuous, the scheme remains second-order accurate.

For the purpose of switching between (1.6) and (1.14), we consider a zone to be inside a discontinuity if a finite difference approximation to the third derivative of the solution is sufficiently large, and if a finite difference approximation to the second derivative changes sign across the zone. In addition, we require that finite difference approximations to the first and third derivatives of the solution near the discontinuity have opposite signs. This last condition causes small plateaus within a general increase or decrease in the solution not to be taken for discontinuities. Finally, we do not apply detection to discontinuities with very small jumps.

The rule by which we switch is given by

$$
a_{L,j} \to a_{L,j}(1 - \eta_j) + a^d_{L,j}\eta_j, \qquad a_{R,j} \to a_{R,j}(1 - \eta_j) + a^d_{R,j}\eta_j. \tag{1.15}
$$

Here η_j is defined by

$$
\eta_j = \max(0, \min(\eta^{(1)}(\tilde{\eta}_j - \eta^{(2)}), 1)), \tag{1.16}
$$

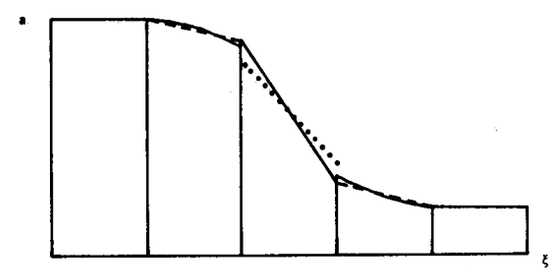

FIG. 3. PPM discontinuity detection. The central zone in this figure is judged to be within a discontinuity, according to the detection criterion given in Eqs. (1.15)–(1.17) of the text. The usual interpolated zone structure shown by the dotted line is therefore replaced by the steeper structure shown by the solid line. The two edge values joined by this line are obtained from the linear distributions in the neighboring zones, which are indicated by the dashed lines. A monotonicity constraint on these linear distributions has kept their slopes small and caused the distribution derived for the central zone to be quite steep.

where

$$\tilde{\eta}_j = -\left(\frac{\delta^2 a_{j+1} - \delta^2 a_{j-1}}{\xi_{j+1} - \xi_{j-1}}\right)\left(\frac{(\xi_j - \xi_{j-1})^3 + (\xi_{j+1} - \xi_j)^3}{a_{j+1} - a_{j-1}}\right)$$

$$\text{if } -\delta^2 a_{j+1} \cdot \delta^2 a_{j-1}, |a_{j+1} - a_{j-1}| - \varepsilon \min(|a_{j+1}|, |a_{j-1}|) > 0$$

$$= 0 \qquad \text{otherwise,}$$

and where

$$\delta^2 a_j = \frac{1}{\Delta\xi_{j-1} + \Delta\xi_j + \Delta\xi_{j+1}}\left[\frac{a_{j+1} - a_j}{\Delta\xi_{j+1} + \Delta\xi_j} - \frac{a_j - a_{j-1}}{\Delta\xi_j + \Delta\xi_{j-1}}\right]. \tag{1.17}$$

The parameters $\eta^{(1)}$, $\eta^{(2)}$ are constants which determine a continuous switch between the schemes (1.6) and (1.14). The parameter ε determines how large a relative change in the solution across a zone one wishes to call a discontinuity. In the calculations shown in [2], we have taken $\eta^{(1)} = 20$, $\eta^{(2)} = 0.05$, $\varepsilon = 0.01$. In gas dynamics calculations, the detection algorithm is applied only to the density interpolation, and only to discontinuities which are contact discontinuities (see Eq. (3.2)).

2. Lagrangian Hydrodynamics

The approach we will take to extending the advection algorithm in the previous section to the equations of gas dynamics in Lagrangian coordinates consists of the following three steps: (1) the interpolation of distributions of the dependent variables, (2) the calculation at the zone edges of the solution as a function of time to the initial value problem implied by the interpolated distributions, using characteristic equations and Riemann solvers, and (3) the use of these solutions to calculate effective fluxes, which are differenced conservatively. It is possible to perform this calculation in such a way that the third-order accuracy in space and time of the advection algorithm is preserved; however, this requires numerous solutions of the Riemann problem, and is therefore rather expensive. In the following, we present a simpler approach, following a suggestion of van Leer [9]. In this approach we sacrifice third-order accuracy in time to the extent that the nonlinear interaction between the two hydrodynamic waves is calculated only to second order. However, we retain the spatial accuracy and the steep representation of the discontinuities of the advection scheme. Test calculations involving strong shocks have shown that there is very little accuracy lost in using the approach described here rather than the third-order-accurate formulation.

We write the equations of gas dynamics in Lagrangian coordinates in conservation form:

$$\begin{aligned} &\frac{\partial \tau}{\partial t} - \frac{\partial (r^\alpha u)}{\partial m} = 0 \\ &\frac{\partial u}{\partial t} + r^\alpha \frac{\partial p}{\partial m} = g \\ &\frac{\partial E}{\partial t} + \frac{\partial (r^\alpha u p)}{\partial m} = ug. \end{aligned} \tag{2.1}$$

Here τ is the specific volume, u is the velocity, E the total energy per unit volume, g a body force depending on r and t, and m a mass coordinate. The internal energy e, the density ρ, and the pressure p are derived from the conserved quantities via

$$\rho = 1/\tau, \qquad e = E - u^2/2, \qquad p = (\gamma - 1)\rho e.$$

Here γ, the ratio of specific heats, is assumed to be a constant greater than 1. The spatial coordinate r is related to the mass coordinate m via

$$m(r) = \int_{r_0}^{r} \rho(r)\, r^\alpha dr, \tag{2.2}$$

where $\alpha = 0, 1, 2$ depending on whether there is planar, cylindrical, or spherical symmetry, respectively. The function $r(m, t)$ satisfies the ordinary differential equation $dr/dt = u(m, t)$.

Let Δm_j be the amount of mass contained in the jth zone. We assume that we know the mass-weighted averages of the conserved quantities at time t^n:

$$U_j^n = \frac{1}{\Delta m_j}\int_{m_{j-1/2}}^{m_{j+1/2}} U(m, t^n)\, dm$$

$$U = \begin{pmatrix} \tau \\ u \\ E \end{pmatrix} \tag{2.3}$$

$$m_{j+1/2} = \sum_{k<j} \Delta m_k.$$

It is also convenient to define $r_{j+1/2}^n = r(m_{j+1/2}, t^n)$ as a separate dependent variable, given by

$$\frac{(r_{j+1/2}^n)^{\alpha+1} - (r_{j_0-1/2}^n)^{\alpha+1}}{\alpha+1} = \sum_{j_0<k<j} \tau_k^m \Delta m_k. \tag{2.4}$$

Then we wish to calculate U_j^{n+1}, the average values for the conserved quantities at time $t^{n+1} = t^n + \Delta t$. The method we are about to describe is a direct extension of Godunov's first-order method which takes into account the correct domain of depen-

dence of zone edges in calculating the conservative fluxes. This is done in the following three steps. We interpolate profiles for the approximate dependent variables τ, u, p as functions of the mass coordinate m, using the interpolation algorithm described in the preceding section. We then solve appropriate Riemann problems (shock tube problems) to calculate the time-averaged pressures and velocities at the edges of zones. Finally, we update the conserved quantities by applying the forces implied by the time-averaged pressures and velocities at the zone edges.

The interpolation step is a straightforward application of the algorithm described in Section 1, with the mass coordinate taking the role of the independent variable ξ. We know Δm_j, the mass increments, and τ_j^n and u_j^n, the mass-weighted averages of τ and u across each zone; so the interpolation coefficients are as in (1.6). The third quantity we interpolate is the pressure p, rather than the total energy, E. The reason for interpolating pressure is that by applying the monotonicity constraints built into the interpolation algorithm to the pressure profile directly, we obtain a better-behaved solution near shocks. We take our average value of the pressure in the zone to be the pressure evaluated from the averages of the conserved quantities: $p_j^n = p(E_j^n, u_j^n, \tau_j^n)$. This is a second-order-accurate value for the average of the pressure across the zone. Given p_j^n, then the interpolation scheme for the pressure is the same as for the other two variables. We do not apply the discontinuity detection algorithm (1.16)–(1.18) to the interpolation of any of the variables, since contact discontinuities automatically remain sharp in Lagrangian calculations.

In the second step, we wish to obtain $\bar{u}_{j+1/2}$ and $\bar{p}_{j+1/2}$, time-averaged values for the velocity and pressure at the edges of zones. These values will be used to compute fluxes which are differenced in an approximation to the conservation laws (2.1). In smooth regions, $\bar{u}_{j+1/2}$ and $\bar{p}_{j+1/2}$ approximate time averages to the solution of the equations in characteristic form:

$$(1/r^\alpha)\, d(r^\alpha u) \pm dp/C = g\,dt \qquad \text{along} \quad dm = \pm r^\alpha C\, dt, \tag{2.5}$$

where $C = (\gamma p \rho)^{1/2}$. The derivation of these equations is standard (e.g., see [10]).

We obtain the values $\bar{u}_{j+1/2}$ and $\bar{p}_{j+1/2}$ by first calculating averages of the dependent variables over the spatial domains which can influence the zone edge during the time step (Figs. 4a, b). The interaction of these averaged states is calculated by solving a Riemann problem for $\bar{u}_{j+1/2}$ and $\bar{p}_{j+1/2}$ (Fig. 4c). The construction of these averaged states is done so that $\bar{u}_{j+1/2}$ and $\bar{p}_{j+1/2}$ satisfy an averaged form of the characteristic equations (2.5) in smooth flow, and are well-behaved at shocks.

We now describe the algorithm for calculating $\bar{u}_{j+1/2}$ and $\bar{p}_{j+1/2}$ in detail. We consider first the case of planar symmetry, and no body forces ($\alpha = g = 0$). We define $\tau_{j+1/2}^{\pm}, u_{j+1/2}^{\pm}, p_{j+1/2}^{\pm}$, the average values of the dependent variables over the region between $m_{j+1/2}$, and the point where the $\pm$ characteristic through $(m_{j+1/2}, t^{n+1})$ intersects the line $\{t = t^n\}$:

$$\begin{aligned} a_{j+1/2}^{+} &= f_{j+1/2,L}^{a}(\Delta t C_j^n A_j^n) \\ a_{j+1/2}^{-} &= f_{j+1/2,R}^{a}(\Delta t C_{j+1}^n A_{j+1}^n), \end{aligned} \tag{2.6}$$

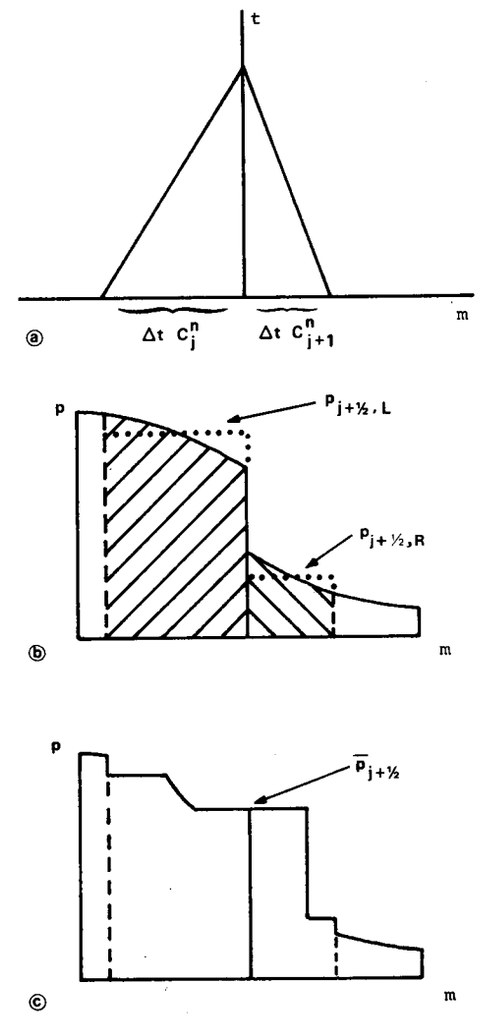

FIG. 4. The computation of Lagrangian fluxes with PPM. (a) The two domains of dependence for a zone interface during the time step are determined by tracing the paths of sound waves arriving at the interface at the end of the time step. (b) The detailed interpolated distribution of each variable within each domain of dependence is replaced by its mass-weighted average. This replacement facilitates the computation of the nonlinear interaction of the two domains of dependence. (c) The interaction of the two averaged states adjacent to the interface is described by a solution to Riemann's shock tube problem. Such a solution is indicated here. The nonlinear waves moving away from the interface reach the edges of the averaged domains at the end of the time step. The Lagrangian fluxes needed to update the zone volume, momentum, and energy are obtained from the parameters of the constant state at the zone interface.

where $a = p, \tau, u$, and

$$A_j^n = \frac{(r_{j+1/2}^n)^{\alpha+1} - (r_{j-1/2}^n)^{\alpha+1}}{(\alpha+1)(r_{j+1/2}^n - r_{j-1/2}^n)}. \tag{2.7}$$

We obtain $\bar{p}_{j+1/2}$ and $\bar{u}_{j+1/2}$ by solving a Riemann problem with left and right states $a_{j+1/2,L} = a_{j+1/2}^+$ and $a_{j+1/2,R} = a_{j+1/2}^-$, where $a = \tau, u, p$. Thus we perform the same procedure here as for Godunov's method to obtain numerical fluxes, except that we construct our left and right states to be the averages over only the parts of each of the zones to the left and right of $m_{j+1/2}$ which are in the domain of dependence of $m_{j+1/2}$ for the time interval (t^n, t^{n+1}). This yields values for $\bar{p}_{j+1/2}$ and $\bar{u}_{j+1/2}$, which satisfy the following nonlinear equations:

$$\begin{aligned}
&\frac{\bar{p}_{j+1/2} - p_{j+1/2,L}}{W_L} + (\bar{u}_{j+1/2} - u_{j+1/2,L}) = 0 \\
&W_L^2 = \left(\frac{\gamma p_{j+1/2}^+}{\tau_{j+1/2}^+}\right)\left(1 + \frac{\gamma+1}{2\gamma}\left(\frac{\bar{p}_{j+1/2}}{p_{j+1/2,L}} - 1\right)\right) \\
&\frac{\bar{p}_{j+1/2} - p_{j+1/2,R}}{W_R} - (\bar{u}_{j+1/2} - u_{j+1/2,R}) = 0 \\
&W_R^2 = \left(\frac{\gamma p_{j+1/2}^-}{\tau_{j+1/2}^-}\right)\left(1 + \frac{\gamma+1}{2\gamma}\left(\frac{\bar{p}_{j+1/2}}{p_{j+1/2,R}} - 1\right)\right).
\end{aligned} \tag{2.8}$$

In order to solve these equations, we use the Newton's method algorithm discussed in [5] with a fixed number of iterations. It is immediately clear that, in smooth parts of the solution, Eqs. (2.8) are a finite difference approximation to the characteristic equations (2.5) which yield time-centered values for $\bar{p}_{j+1/2}$ and $\bar{u}_{j+1/2}$. In the neighborhood of strong discontinuities, we retain the advantages of using the Riemann problem to calculate fluxes.

In order to calculate $\bar{u}_{j+1/2}$ and $\bar{p}_{j+1/2}$ in the case where a body force or nonplanar symmetry is present, we look for a modified definition of $p_{j+1/2,L}$, $u_{j+1/2,L}$, $p_{j+1/2,R}$, $u_{j+1/2,R}$ such that Eqs. (2.8) are still a finite difference approximation to the characteristic equations. If we define

$$\begin{aligned}
p_{j+1/2,L} &= p_{j+1/2}^+ + \Delta t C_{j+1/2}^+ g_j^n, & u_{j+1/2,L} &= u_{R,j} + \frac{A_{j+1/2}^+ u_{j+1/2}^+ - A_{j+1/2} u_{R,j}}{\frac{1}{2}(A_{j+1/2}^+ + A_{j+1/2})} \\
p_{j+1/2,R} &= p_{j+1/2}^- - \Delta t C_{j+1/2}^- g_{j+1}^n, & u_{j+1/2,R} &= u_{L,j+1} + \frac{A_{j+1/2}^- u_{j+1/2}^- - A_{j+1/2} u_{L,j+1}}{\frac{1}{2}(A_{j+1/2}^- + A_{j+1/2})}
\end{aligned} \tag{2.9}$$

then Eqs. (2.8) are again finite difference approximations to (2.5) which yield time-centered values for $\bar{p}_{j+1/2}$ and $\bar{u}_{j+1/2}$. Here $A_{j+1/2}^{\pm}$ are defined in the same way as the other dependent variables, with the interpolation coefficients for $A(r) = r^\alpha$ given by

(1.5), $A_{R,j} = A_{L,j+1} = A_{j+1/2} = (r_{j+1/2}^n)^\alpha$, and A_j^n given by Eq. (2.7). The interpolation of A is performed in the mass coordinate. In the case where $\alpha = g = 0$, this procedure for calculating the fluxes reduces to the one previously discussed. This modification technique has the property that, in the case where the initial data is a smooth steady solution to the equations of motion, then the effective left and right states differ from one another by terms of second order. Thus we do not introduce a false jump into the Riemann problem which might give rise to spurious transients.

The final difference approximation to the fundamental conservation laws in Eqs. (2.1) is as follows:

$$\begin{aligned}
&r_{j+1/2}^{n+1} = r_{j+1/2}^n + \Delta t \bar{u}_{j+1/2}, \qquad \bar{A}_{j+1/2} = \frac{(r_{j+1/2}^{n+1})^{\alpha+1} - (r_{j+1/2}^n)^{\alpha+1}}{(\alpha+1)\,\bar{u}_{j+1/2}\Delta t} \\
&\tau_j^{n+1} = \frac{(r_{j+1/2}^{n+1})^{\alpha+1} - (r_{j-1/2}^{n+1})^{\alpha+1}}{(\alpha+1)\,\Delta m_j} \\
&u_j^{n+1} = u_j^n + \frac{1}{2}(\bar{A}_{j+1/2} + \bar{A}_{j-1/2})\frac{\Delta t}{\Delta m_j}(\bar{p}_{j-1/2} - \bar{p}_{j+1/2}) + \frac{\Delta t}{2}(g_j^n + g_j^{n+1}) \\
&E_j^{n+1} = E_j^n + \frac{\Delta t}{\Delta m_j}(\bar{A}_{j-1/2}\bar{u}_{j-1/2}\bar{p}_{j-1/2} - \bar{A}_{j+1/2}\bar{u}_{j+1/2}\bar{p}_{j+1/2}) \\
&\qquad + \frac{\Delta t}{2}(u_j^n g_j^n + u_j^{n+1} g_j^{n+1}).
\end{aligned} \tag{2.10}$$

The appearance of u_j^{n+1} in the equation for the energy does not make the calculation implicit, since u_j^{n+1} does not depend on E_j^{n+1}.

This completes our discussion of the PPM Lagrangian scheme. Given a one-dimensional Lagrangian method, and an advection scheme of the type discussed in the previous section, it is straightforward to combine them into a one-dimensional Eulerian algorithm by performing a Lagrangian step, and remapping the results back onto the fixed Eulerian grid. This two-step technique, first proposed by Noh, has been in widespread use for some time; therefore, we will not discuss it in detail here (for an example of how such a scheme is implemented for methods of this type, see [5]). There are, however, a number of minor modifications which must be made to the algorithms discussed in this section and the previous one so that the resulting Eulerian method is well-behaved. First, all the interpolations for both the Lagrangian step and the remap must be performed in the volume coordinate $r^{\alpha+1}/(\alpha+1)$, rather than in the mass coordinate. In particular, the density, rather than the specific volume, is interpolated for the Lagrangian step. Second, the total energy interpolation for the remap must be performed by interpolating values at the edges of zones for p, ρ, u; then, the total energy per unit mass at a zone edge is given by $E_{j+1/2} = p_{j+1/2}/((\gamma-1)\rho_{j+1/2}) + \frac{1}{2}u_{j+1/2}^2$. These values are then used, along with the values of the conserved total energy, to construct interpolated distributions of total energy using (1.6) and (1.10), which are then remapped in the usual fashion. Both of

these modifications are necessary in order to maintain consistency between the Lagrangian step and the remap. Finally, the discontinuity detection algorithm (1.15)–(1.17) is applied to the density interpolation for the remap, subject to the additional constraint that it be applied only at density jumps corresponding to contact discontinuities. A criterion for detecting such jumps is given in the next section (Eq. (3.2)).

3. Eulerian Hydrodynamics

We will be calculating solutions to the equations of compressible hydrodynamics in one space variable, written in conservation form:

$$\frac{\partial U}{\partial t}+\frac{\partial(AF)}{\partial V}+\frac{\partial H}{\partial r}=G$$

$$U=\begin{pmatrix}\rho\\ \rho u\\ \rho v\\ \rho E\end{pmatrix},\quad F(U)=\begin{pmatrix}\rho u\\ \rho u^2\\ \rho uv\\ \rho uE+up\end{pmatrix},\quad H(U)=\begin{pmatrix}0\\ p\\ 0\\ 0\end{pmatrix},\quad G=\begin{pmatrix}0\\ \rho g\\ 0\\ \rho ug\end{pmatrix}. \tag{3.1}$$

Here $V(r)=r^{\alpha+1}/(\alpha+1)$ is a volume coordinate, $A(r)=r^{\alpha}$. The notation here is that of the previous section, except that u is the component of velocity in the direction of the one-dimensional sweep, v the velocity orthogonal to u (hereafter, u and v will be referred to, respectively, as the velocity and transverse velocity), and that we define e, the internal energy per unit mass, to be $E-\frac{1}{2}(u^2+v^2)$.

Let $r_{j+1/2}$ be the boundary between zones j and $j+1$; we define $\Delta r_j=r_{j+1/2}-r_{j-1/2}$ and $\Delta V_j=V(r_{j+1/2})-V(r_{j-1/2})$. We assume that, at time t^n, we know $U_j^n=(1/\Delta V_j)\int_{r_{j-1/2}}^{r_{j+1/2}}U(r,t^n)\,dV$, the volume-weighted average values of the conserved quantities in the interval $(r_{j-1/2},r_{j+1/2})$; then we wish to calculate U_j^{n+1}, the averages of the conserved quantities at time $t^{n+1}=t^n+\Delta t$. The construction of the single-step Eulerian scheme for performing such a calculation has the same basic structure as the Lagrangian scheme: we interpolate piecewise parabolic distributions of the dependent variables, construct effective left and right states for Riemann problems, and difference fluxes determined by the solution to those Riemann problems. The construction of the effective left and right states for the Riemann problems is more complicated than in the Lagrangian case, since there can be as many as three characteristics, or as few as none, reaching the edge of a zone from a given side. One approach to this difficulty is to use a construction similar to that used in [7] for solving the characteristic equations in the single-step Eulerian MUSCL. In the following, we shall describe a different approach, in which we construct a first guess to the left and right states using the largest and smallest values of the characteristic speeds; this first guess is then corrected using the linearized characteristic equations.

First, we derive interpolation functions $a(V)$, using the interpolation scheme described in Section 1, given $a_j^n=a(U_j^n)$, $a=p,\rho,u,v$, and interpolating with respect to the volume coordinate V. As was the case for the pressure interpolation for the Lagrangian scheme, the approximation that u_j^n, v_j^n, p_j^n are the averages with respect to V of the velocities and the pressure across the zone is second-order accurate. We use the interpolation scheme without discontinuity detection for the quantities p, u, v; for ρ, we use the interpolation scheme with discontinuity detection, with the modification that that we do not treat the jth zone as being inside a discontinuity unless the following condition is also satisfied:

$$\gamma K_0\frac{|\rho_{j+1}-\rho_{j-1}|}{\min(\rho_{j+1},\rho_{j-1})}\geqslant\frac{|p_{j+1}-p_{j-1}|}{\min(p_{j+1},p_{j-1})}. \tag{3.2}$$

This is to ensure that the special interpolation at a detected discontinuity is only applied at jumps which are predominantly contact discontinuities. Here K_0 is a constant, which is problem dependent; in the calculations in [2], $K_0=0.1$.

Using these interpolation functions, we can now define $\tilde{a}_{j+1/2,L}$ and $\tilde{a}_{j+1/2,R}$, our first guess at the effective left and right states of the Riemann problem. We define them to be

$$\begin{gathered}\tilde{a}_{j+1/2,L}=f^a_{j+1/2,L}(V_{j+1/2}-V(\tilde{r}_{j+1/2,L})),\quad \tilde{r}_{j+1/2,L}=r_{j+1/2}-\max(0,\Delta t(u_j^n+c_j^n))\\ \tilde{a}_{j+1/2,R}=f^a_{j+1/2,R}(V(\tilde{r}_{j+1/2,R})-V_{j+1/2}),\quad \tilde{r}_{j+1/2,R}=r_{j+1/2}+\max(0,-\Delta t(u_{j+1}^n-c_{j+1}^n))\\ a=p,\rho,u,v.\end{gathered} \tag{3.3}$$

Thus $\tilde{a}_{j+1/2,L}$ ($\tilde{a}_{j+1/2,R}$) is the average over that part of the domain of dependence of $r_{j+1/2}$ for the time interval (t^n,t^{n+1}) which lies to the left (right) of $r_{j+1/2}$. If there are no characteristics impinging on $r_{j+1/2}$ from the left (right), then $\tilde{a}$ is taken to be the left (right) limit of the interpolation function at $r_{j+1/2}$ (Fig. 5).

As they stand, the states constructed above are not suitable as left and right states for the Riemann problem. For example, if $\alpha=g=0$, and if the only variation in the solution were a density gradient carried by a positive constant velocity field, then the use of the above states for the Riemann problem would imply that the amount of mass which crosses $r_{j+1/2}$ during the time step would be

$$\frac{u_j^n}{u_j^n+c_j^n}\int_{r_{j+1/2}-\Delta t(u_j^n+c_j^n)}^{r_{j+1/2}}\rho(r)\,dr.$$

This differs from $\int_{r_{j+1/2}-\Delta t u_j^n}^{r_{j+1/2}}\rho(r)\,dr$, the answer obtained in Section 1 for this problem, by terms which are $O(c_j^n\Delta t\Delta r_j))$, making the scheme first-order accurate for the special case of advection. Therefore, we must make some correction to take into account the fact that there can be more than one wave moving in each direction. The corrected left and right states are to be constructed in such a way that the amount of

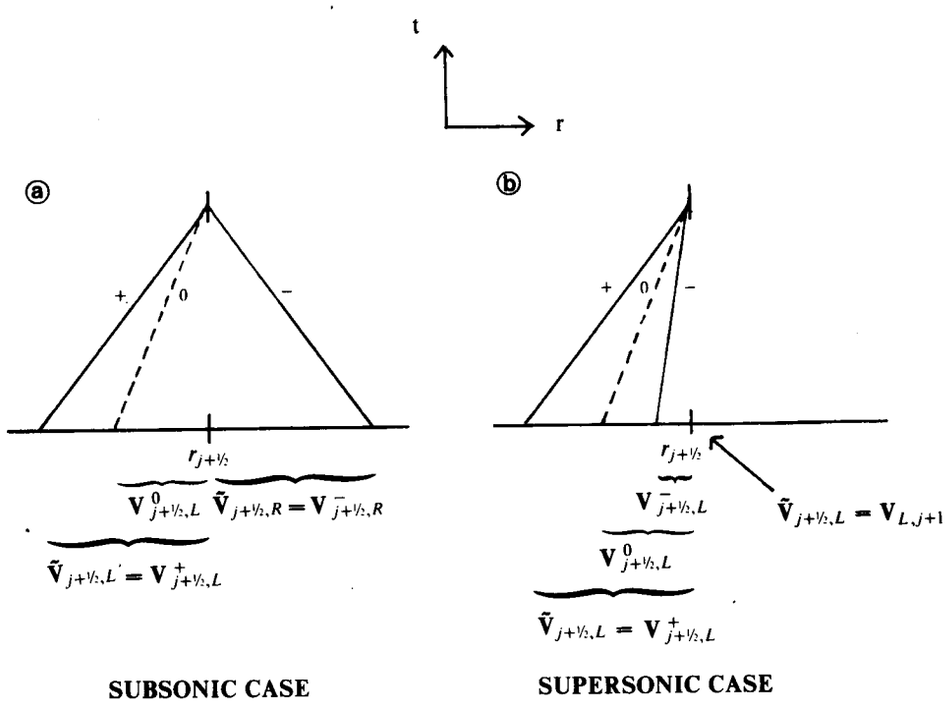

FIG. 5. The locations of the characteristic domains of dependence referred to in the construction of effective left- and right-hand states for the Riemann problem in the single-step Eulerian formulation of PPM. The characteristics labelled with + and − are the paths traversed by sound waves travelling to the right and left with respect to the fluid. The dashed characteristics are fluid streamlines. The other symbols in the figure are defined in the text.

wave associated with each family of characteristics transported across a zone edge is correct up to terms of second order. Furthermore, we require that in the absence of pressure and velocity gradients the fluxes be exactly those given by the advection algorithm discussed in Section 1.

We correct our initial guess for the left and right states by solving the equations of gas dynamics in characteristic form. We consider the equations of gas dynamics in one space variable, written in nonconservation form.

$$\frac{\partial \mathbf{V}}{\partial t} + \mathbf{A}\frac{\partial \mathbf{V}}{\partial r} + \mathbf{G} = 0 \tag{3.4}$$

$$\mathbf{V} = \begin{pmatrix} \rho \\ u \\ p \end{pmatrix}, \qquad \mathbf{A}(\mathbf{V}) = \begin{pmatrix} u & \rho & 0 \\ 0 & u & \tau \\ 0 & \rho c^2 & u \end{pmatrix}, \qquad \mathbf{G}(\mathbf{V}, r, t) = \begin{pmatrix} \dfrac{\alpha\rho u}{r} \\ -g \\ \dfrac{\alpha c^2 \rho u}{r} \end{pmatrix}.$$

Then $\mathbf{A}$ has left and right eigenvectors $(\mathbf{l}_-(\mathbf{V}), \mathbf{r}_-(\mathbf{V}))$, $(\mathbf{l}_0(\mathbf{V}), \mathbf{r}_0(\mathbf{V}))$, $(\mathbf{l}_+(\mathbf{V}), \mathbf{r}_+(\mathbf{V}))$, with associated eigenvalues $\lambda_- = u - c$, $\lambda_0 = u$, and $\lambda_+ = u + c$. The normalization of the eigenvectors can be chosen such that $\mathbf{l}_\# \cdot \mathbf{r}_{\#'} = \delta_{\#,\#'}$, $\#, \#' = +, -, 0$. In this notation, we are given $\tilde{\mathbf{V}}_{j+1/2,L}$ and $\tilde{\mathbf{V}}_{j+1/2,R}$ from (3.3); and we wish to calculate $\mathbf{V}_{j+1/2,L}$ and $\mathbf{V}_{j+1/2,R}$, effective left and right states for the Riemann problem.

First, we define

$$\begin{aligned} a^\#_{j+1/2,L} &= f^a_{j+1/2,L}(V_{j+1/2} - V(r^\#_{j+1/2,L})), & r^\#_{j+1/2,L} &= r_{j+1/2} - \Delta t \lambda_\#(U^n_j) \\ a^\#_{j+1/2,R} &= f^a_{j+1/2,R}(V(r^\#_{j+1/2,R}) - V_{j+1/2}), & r^\#_{j+1/2,R} &= r_{j+1/2} - \Delta t \lambda_\#(U^n_{j+1}) \end{aligned} \tag{3.5}$$

$$a = p, \rho, u.$$

If $\lambda_\#(U^n_j) > 0$ ($\lambda_\#(U^n_j) < 0$), then $\mathbf{V}^\#_{j+1/2,L}$ ($\mathbf{V}^\#_{j+1/2,R}$) is the average of $\mathbf{V}$ over the part of the domain of dependence for the $\#$-characteristic of $r_{j+1/2}$ for the time interval (t^n, t^{n+1}) which lies to the left (right) of $r_{j+1/2}$. We then obtain, for example, $\mathbf{V}_{j+1/2,L}$ by subtracting from $\tilde{\mathbf{V}}_{j+1/2,L}$ the quantity $\mathbf{l}_\# \cdot (\tilde{\mathbf{V}}_{j+1/2,L} - \mathbf{V}^\#_{j+1/2,L} + \Delta t \mathbf{G})\, \mathbf{r}_\#$, for each family of waves for which $\lambda_\#(U^n_j)$ is positive. In the case $\mathbf{G} = 0$, we are subtracting from $\tilde{\mathbf{V}}_{j+1/2,L}$ the amount of wave of the $\#$ family contained in the difference $\tilde{\mathbf{V}}_{j+1/2,L} - \mathbf{V}^\#_{j+1/2,L}$. This is the appropriate nonlinear generalization of subtracting from $\tilde{\mathbf{V}}_{j+1/2,L}$ the amount of wave in the $\#$ family contained in $\tilde{\mathbf{V}}_{j+1/2,L}$ which will not reach $r_{j+1/2}$ by the time $t^n + \Delta t$. When source terms are present, we are modifying $\tilde{\mathbf{V}}_{j+1/2,L}$ to properly account for all the characteristic information impinging on $r_{j+1/2}$ from the left. In particular, if $u^n_j > c^n_j$, $\mathbf{V}_{j+1/2,L}$ is a solution to the characteristic form of Eqs. (3.4) at $(r_{j+1/2}, t^n + \frac{1}{2}\Delta t)$ which is correct to terms of $O(\Delta r_j \Delta t)$ if the variation in the solution across the zone is $O(\Delta r_j)$. A similar construction can be performed for $\mathbf{V}_{j+1/2,R}$. The result of this construction for both sides, modified slightly for the present application, is the following:

$$\begin{aligned} p_{j+1/2,S} &= \tilde{p}_{j+1/2,S} + \tilde{C}^2_{j+1/2,S}(\beta^+_{j+1/2,S} + \beta^-_{j+1/2,S}) \\ u_{j+1/2,S} &= \tilde{u}_{j+1/2,S} + \tilde{C}_{j+1/2,S}(\beta^+_{j+1/2,S} - \beta^-_{j+1/2,S}) \\ \rho_{j+1/2,S} &= \left(\frac{1}{\tilde{\rho}_{j+1/2,S}} - \sum_{\#=0,+,-} \beta^\#_{j+1/2,S}\right)^{-1}. \end{aligned} \tag{3.6}$$

Here, $\tilde{C}^2_{j+1/2,S} = \gamma \tilde{p}_{j+1/2,S} \tilde{\rho}_{j+1/2,S}$, and $S = L, R$. We also have

$$\begin{aligned} v_{j+1/2,L} &= \tilde{v}_{j+1/2,L}, & \beta^\#_{j+1/2,L} &= 0 \quad \text{if} \quad \lambda_\#(U^n_j) \leqslant 0 \\ v_{j+1/2,R} &= \tilde{v}_{j+1/2,R}, & \beta^\#_{j+1/2,R} &= 0 \quad \text{if} \quad \lambda_\#(U^n_{j+1}) \geqslant 0. \end{aligned}$$

Otherwise

$$\beta^{\pm}_{j+1/2,s} = \mp \frac{1}{2\tilde{C}_{j+1/2,s}} \times \left((\tilde{u}_{j+1/2,s} - u^{\pm}_{j+1/2,s}) \pm \frac{(\tilde{p}_{j+1/2,s} - p^{\pm}_{j+1/2,s})}{\tilde{C}_{j+1/2,s}} \pm \Delta t \left(\frac{a u^{+}_{j+1/2,s} c^{\pm}_{j+1/2,s}}{r^{\pm}_{j+1/2,s}} \mp g^{\pm}_{j+1/2,s} \right) \right) \tag{3.7}$$

$$\beta^{0}_{j+1/2,s} = \left(\frac{(\tilde{p}_{j+1/2,s} - p^{0}_{j+1/2,s})}{\tilde{C}^{2}_{j+1/2,s}} + \frac{1}{\tilde{\rho}_{j+1/2,s}} - \frac{1}{\rho^{0}_{j+1/2,s}} \right)$$

$$v_{j+1/2,s} = v^{0}_{j+1/2,s}.$$

We have taken advantage of the fact that ρ is the natural variable to interpolate, while $\tau = 1/\rho$ is the natural variable for the characteristic equations. We have also exploited the decoupling of the equation for the transverse velocity from the rest of the equations when they are written in nonconservation form.

To obtain $\bar{U}_{j+1/2}$, an approximation to $(1/\Delta t)\int_{t^n}^{t^{n+1}} U(r_{j+1/2}, t)\, dt$, the time-averaged value of the solution at $r_{j+1/2}$, we solve the Riemann problem at $r_{j+1/2}$ with left and right states

$$(\rho_{j+1/2,L}, p_{j+1/2,L}, u_{j+1/2,L}, v_{j+1/2,L})$$
$$(\rho_{j+1/2,R}, p_{j+1/2,R}, u_{j+1/2,R}, v_{j+1/2,R}).$$

We use the Riemann problem solver for the Cartesian equations here; the effect of the source terms on $\bar{U}_{j+1/2}$ is accounted for to second order in the construction of $\mathbf{V}_{j+1/2,L}$, $\mathbf{V}_{j+1/2,R}$. The Riemann solver we used for the calculations shown in [2] uses the same iteration scheme as that described above for the Lagrangian PPM; the evaluation of the solution at $r_{j+1/2}$ is performed in the usual fashion, except that the evaluation of the solution inside of a rarefaction fan is done by linear interpolation between the states on either side of the fan.

The final conservative difference step is given by

$$U^{n+1}_j = U^n_j + \Delta t \left(\frac{A_{j-1/2} F(\bar{U}_{j-1/2}) - A_{j+1/2} F(\bar{U}_{j+1/2})}{\Delta V_j} + \frac{H(\bar{U}_{j-1/2}) - H(\bar{U}_{j+1/2})}{\Delta r_j} \right) + \bar{G}_j \Delta t$$

$$A_{j+1/2} = A(r_{j+1/2}), \qquad \bar{G}_j = \frac{1}{2} \begin{pmatrix} 0 \\ (\rho^n_j g^n_j + \rho^{n+1}_j g^{n+1}_j) \\ 0 \\ (\rho^n_j u^n_j g^n_j + \rho^{n+1}_j u^{n+1}_j g^{n+1}_j) \end{pmatrix}. \tag{3.8}$$

The above definition of $\bar{G}_j$ does not make the method implicit, inasmuch as the values of ρ^{n+1} do not depend upon u^{n+1}; nor do those of $\rho^{n+1}u^{n+1}$ depend upon E^{n+1}.

4. Dissipation Mechanisms

In [2] and [7], low-amplitude post-shock oscillations were observed in calculations performed with the single-step Eulerian MUSCL scheme for shocks whose speed was small relative to the post-shock characteristic speed. Unless extra dissipation is added, the same type of noise occurs when the PPM scheme is formulated either as a Lagrangian step followed by a remap or as a single Eulerian step. In this section, we will describe in detail the circumstances under which noise is present, and discuss the types of dissipation employed in the calculations in [2] using the PPM scheme to reduce or eliminate the noise. We shall discuss these issues in general terms in this section; in an Appendix, we will give detailed algorithms for the dissipation schemes used in the PPM calculations in [2].

In Fig. 6, we show a typical example of the type of errors which are observed. This figure shows the results of a calculation of a very strong planar shock using the Lagrangian PPM scheme described in Section 2. The calculation is quite stable; however, there are substantial oscillations in both the entropy and $u - 2c/(\gamma - 1)$, the Riemann invariant transported along the $-$ characteristic, which crosses the shock. The quantity $u + 2c/(\gamma - 1)$, the Riemann invariant transported along the $+$ characteristic, is quite well-behaved; any errors generated in that variable are immediately driven back into the shock transition layer. This reflects the fact that this difficulty arises only for systems of equations; indeed, these methods produce shocks which are perfectly well-behaved when applied to a scalar equation.

A technique which is successful in eliminating this error in a large number of cases is that of flattening the interpolation profiles in the neighborhood of shocks which are sufficiently strong and steep. In effect, flattening is a means of reducing locally the order of the method; in the limit that the interpolation function is totally flattened, we obtain locally Godunov's first-order method.

We define f_j, $0 \leqslant f_j \leqslant 1$, so that our interpolation function in the jth zone is $a(\xi)(1 - f_j) + f_j a^n_j$, $\xi_j < \xi < \xi_{j+1/2}$, where $a(\xi)$ is the interpolation function defined in Section 1. This is most easily accomplished by defining

$$a^{flat}_{L,j} = a^n_j f_j + a_{L,j}(1 - f_j)$$
$$a^{flat}_{R,j} = a^n_j f_j + a_{R,j}(1 - f_j) \tag{4.1}$$

and substituting $a^{flat}_{L,j}$ and $a^{flat}_{R,j}$ for $a_{L,j}$ and $a_{R,j}$ in (1.5).

The coefficient f_j should be equal to 0 away from strong shocks. Excessive broadening of the shocks is undesirable; consequently, we set f_j to 0 if the shock profile is sufficiently broad. We measure the width of the profile for a shock transition centered on the jth zone by calculating the ratio $(q_{j+1} - q_{j-1})/(q_{j+2} - q_{j-2})$, where q is some variable which jumps across the shock, such as the pressure or energy. If this ratio is sufficiently close to 1, then the profile is considered sufficiently steep for f_i to be nonzero (Fig. 7). For Lagrangian calculations, we have found that we obtain all of the required dissipation when the effective shock width is barely

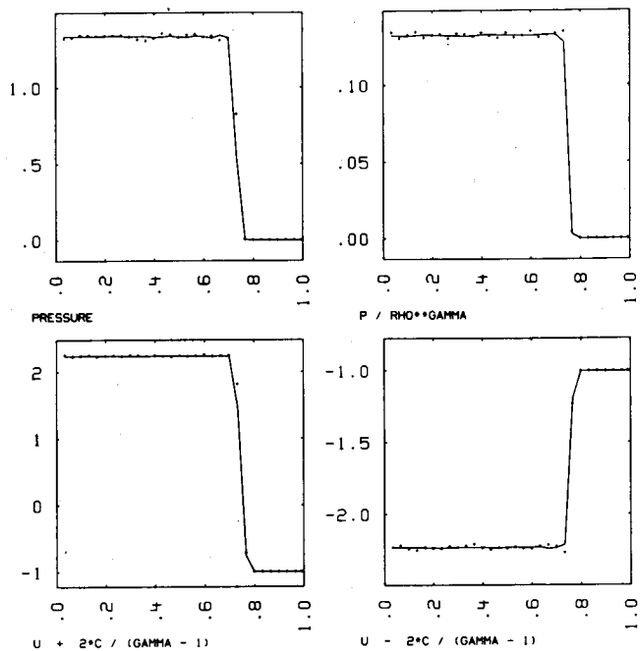

FIG. 6. The results of the Lagrangian PPM scheme for the propagation of an extremely strong isolated shock in a polytropic gas with $\gamma = 5/3$. The pressure jump in the shock exceeds six orders of magnitude. Thirty zones are displayed for two separate calculations. The dots show results of the PPM scheme described in Section 2. Small oscillations of about 1.3% amplitude can be seen in the post-shock flow for this calculation. These oscillations occur mainly in the two Riemann invariants whose associated characteristics cross the shock. The solid lines display results of the PPM scheme augmented by the algorithm for selectively flattening internal zone structures which is described in Section 4. The amplitude of post-shock oscillations has been dramatically reduced by this flattening procedure.

more than one mesh length. We see in Fig. 6 that the flattening nearly eliminates the oscillation behind the shock, while broadening the shock only slightly.

For Eulerian calculations, there are circumstances in which flattening is ineffectual. We present in Fig. 8 a calculation of an extremely strong, nearly stationary shock performed using the single-step Eulerian Godunov method [4]. Even though this is a first-order method, we still see a 3% error in the density immediately behind the shock. The error has disappeared farther downstream from the shock, due to the strongly dissipative character of Godunov's method. No amount of local flattening can eliminate such an error from a higher-order method, since it is still present in calculations performed with a scheme with all the interpolation functions totally flattened. A second kind of error which cannot be effectively eliminated by flattening was observed in the single-step Eulerian MUSCL and Godunov results for the Mach 3 wind tunnel calculation presented in [2]. In the finely zoned runs of that problem,

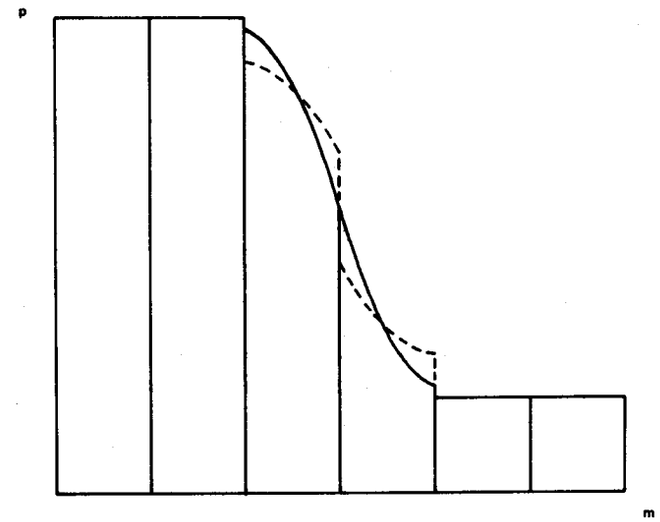

FIG. 7. A shock discontinuity which requires flattening of the internal zone structures within the shock. The solid lines show the internal zone structures interpolated by the PPM algorithm. The dashed lines show these structures after they have been flattened. This flattening procedure eliminates the mild post-shock oscillations displayed in Fig. 6.

we saw oscillations behind the incident shock near the point where the shock intersects the bottom of the channel, and behind the Mach stem.

Both of these errors occur when a characteristic speed associated with a strong shock, measured relative to the grid, vanishes. The dissipation introduced by Godunov's method at a shock, as measured, for example, by the number of mesh points over which the shock is spread, vanishes as the speed of the shock goes to zero. What we are observing in the first example mentioned above is that the residual dissipation present in a slowly moving strong shock calculated using Godunov's method is not sufficient to guarantee the correct entropy production across the shock. In the second example, the component of the velocity tangent to the shock, which is also the velocity in one of the coordinate directions, is nearly zero. In the column of zones where the shock transition occurs, a small disturbance develops in the tangential velocity, due to numerical error. These small velocities transport large amounts of the conserved quantities, creating, in effect, large sources and sinks in the shock transition zone for the essentially one-dimensional calculations of the motion of the shock in each row of zones. Finally, although we have discussed these errors in terms of the single-step Eulerian schemes, they occur as well when the PPM Eulerian scheme is formulated as a Lagrangian step followed by a remap. Thus we must find a means for eliminating these errors for either type of Eulerian calculation.

In order to reduce these errors, we introduce a small amount of additional

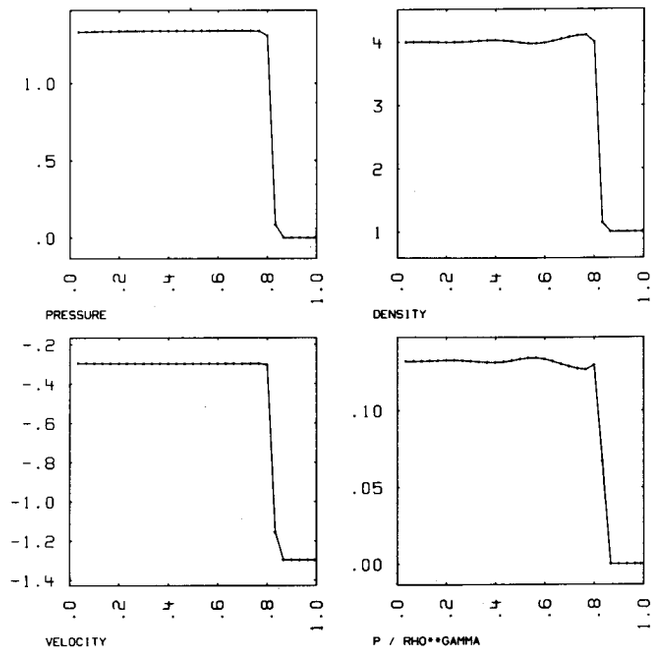

FIG. 8. Results of the propagation of an extremely strong, isolated shock obtained using the single-step Eulerian method of Godunov. The pressure jumps by more than 6 orders of magnitude in the shock, while the velocity jump is unity. The shock is nearly steady; it has taken nearly 8000 time steps to cross 160 zones. Only 30 zones near the shock are displayed, with dots showing the averages of the variables within the zones. Because this shock is strong and nearly stationary, the shock structure is very thin. This causes 3% errors in the entropy of the post-shock gas. Note that this calculation performed 6 iterations in solving each Riemann problem. If only 2 iterations are performed, very large errors are generated in the single zone just behind the shock.

dissipation beyond that which can be obtained by flattening. One way of doing this is to add an explicit diffusive flux to the numerical fluxes.

$$F_{j+1/2} \to F_{j+1/2} + v_{j+1/2}(U_j - U_{j+1}). \tag{4.2}$$

Another way of introducing dissipation is to perform the calculation on a constantly moving grid. If the mesh edges have values $r^n_{j+1/2}$ at time t^n, then

$$\begin{aligned} r^{n+1}_{j+1/2} &= r_{j+1/2} + v_{j+1/2}\Delta t \\ r^{n+2}_{j+1/2} &= r^{n+1}_{j+1/2} - v_{j+1/2}\Delta t = r^n_{j+1/2}. \end{aligned} \tag{4.3}$$

This is equivalent to superimposing an advection velocity to the fluid motion which alternates direction every other time step. The dissipation obtained in this fashion is

that of the PPM advection scheme. This form of dissipation can also be used in operator split multidimensional calculations, as long as two one-dimensional sweeps in succession are performed in each coordinate direction. This is the case, for example, for second-order operator splitting in two dimensions. Then the mesh is aligned properly at the beginning and end of each pair of one-dimensional sweeps.

In both types of dissipation $v_{j+1/2}$ is a velocity which should be large only in the neighborhood of shocks. In one dimension, one might take

$$v_{j+1/2} = K \max(u_j - u_{j+1}, 0). \tag{4.4}$$

In the first example, this yields an artificial viscosity similar to the one used by Lapidus [11]. In more than one dimension, the velocity should be of the form

$$v_{j+1/2,k} = K \max[-(D \cdot \vec{u}^n)_{j+1/2,k}, 0], \tag{4.5}$$

where $(D \cdot \vec{u}^n)_{j+1/2,k}$ is a discrete undivided difference approximation to the multidimensional divergence of $\vec{u}$. It is necessary to use a velocity such as this one, which can detect the presence of a shock jump in the direction perpendicular to that of the one-dimensional sweep, in order to eliminate the multidimensional oscillation discussed above.

The amount of dissipation required is quite small, relative to what is typically used in conventional finite difference schemes. For example, in the results presented in [2], the value of the coefficient K used with (4.2) and (4.5) for the single-step Eulerian PPM was $K = 0.1$, while MacCormack's method needed an artificial viscosity of the form (4.2) and (4.4) with $K = 1$ in order to produce acceptable results. In the case where the dissipation is added by introducing a local grid velocity, the amount of additional dissipation in smooth parts of the flow is even less, even for moderate ($K \sim 1$) values for the grid velocity. This is because the dissipation is essentially that of the PPM advection scheme, which is very small, in smooth parts of the solution. Furthermore, the grid motion itself vanishes with $u_j - u_{j+1}$.

5. DISCUSSION AND CONCLUSIONS

We have presented here the PPM scheme for gas dynamics. Although the scheme is quite complicated, relative to conventional difference methods, we feel that the numerical results in [2] prove that the additional expense and programming effort are worthwhile. Our own investigations indicate that the algorithms presented here are the minimal ones, in the following sense: any further simplifications which we have attempted to introduce into them led to some degradation of the results.

The addition of more complicated physics to this algorithm appears to be quite straightforward. Multifluid capability can be easily added, particularly to the two-step

Eulerian version of the method; the extension of the method to more general equations of state can be done using the techniques described in [12]. These and other extensions of the basic PPM scheme are currently being implemented.

APPENDIX

In this Appendix, we will describe in detail the dissipation algorithms introduced into the PPM scheme for the calculations presented here and in [2]. We will describe three dissipation schemes. The first is a combination of a simplified flattening algorithm and a small amount of artificial viscosity, which was used in all but one of the single-step Eulerian calculations in [2]. The second is a flattening algorithm, suitable for Lagrangian calculation in one dimension. Finally, we will describe a combination of flattening and local mesh motion for use in multidimensional Eulerian calculations which was used in the two-step Eulerian calculations presented in [2] as well as for the single-step Eulerian calculations presented in Fig. 4 of that paper.

Throughout the following, we will use the notation and terminology developed in Section 4. In particular, we will be defining flattening coefficients f_j to be applied in modifying the interpolation functions using (4.1). A quantity we will use throughout this discussion is w_j, which is equal to 1 if the jth zone is inside a pressure and velocity jump in the direction of the sweep consistent with the possibility of there being a shock, and zero elsewhere. Specifically, we will define w_j:

$$\begin{aligned} w_j &= 1 \quad \text{if} \quad \frac{(p_{j+1}-p_{j-1})}{\min(p_{j+1},p_{j-1})} > \varepsilon \text{ and } u_{j-1}-u_{j+1} > 0 \\ &= 0 \quad \text{otherwise.} \end{aligned} \tag{A.1}$$

In all the calculations presented here and in [2], $\varepsilon = 0.33$. Another quantity which we will need is s_j, which is equal to 1 if $p_{j+1}-p_{j-1} < 0$, and is equal to -1 if $p_{j+1}-p_{j-1} > 0$, i.e., the zone $j+s_j$ is the zone just upstream from zone j if zone j is in a shock. In what follows, we assume that two-dimensional calculations are performed on a rectangular grid in one-dimensional sweeps. We denote the coordinate in the direction of the sweep by r, and the coordinate in the direction perpendicular to the sweep by z. We assume we are sweeping through the kth row of zones; the centers of zones are denoted by (r_j, z_k).

The simplest form of dissipation of the types discussed in Section 4 is a flattening based on the steepness of the pressure jump across a zone, plus the addition of a dissipative flux of the form (4.2). Specifically, if we define

$$f_i = \max(\tilde{f}_j, \tilde{f}_{j+s_j}), \tag{A.2}$$

where

$$\tilde{f}_j = 1 - w_j \max\left(0, \left(\frac{p_{j+1}-p_{j-1}}{p_{j+2}-p_{j-2}} - \omega^{(1)}\right)\omega^{(2)}\right);$$

and

$$v_{j+1/2,k} = v^{(1)} \max((u_j - u_{j+1}) + \frac{r_{j+1}-r_j}{2(z_{k+1}-z_{k-1})}((v_{j+1,k-1}+v_{j,k-1}) - (v_{j+1,k+1}+v_{j,k+1})), 0) \tag{A.3}$$

with $\omega^{(1)}$, $\omega^{(2)}$, $v^{(1)}$ constants, then we obtain sufficient dissipation to reduce the errors in all but a few instances to a fraction of a percent in the post-shock values, and to less than two percent in all the cases we tested. The single-step Eulerian calculations presented in [2] used this dissipation algorithm, with the constants set at $\omega^{(1)} = 0.75$, $\omega^{(2)} = 10$, $v^{(1)} = 0.1$.

The defect in this simple approach is twofold: first, it does not totally eliminate the error in all cases; second, it introduces extra dissipation in regions where it is not needed. For this reason, we will introduce dissipation schemes which are more discriminating.

We consider first the case of Lagrangian hydrodynamics. In this case, we can obtain acceptable results by using two parameters: ω_j, which measures the steepness of a shock near j, and κ_j, which depends on the wavelength of any potential noise:

$$\omega_j = \max(0, \omega^{(1)}(\omega^{(2)} - \tilde{\omega}_j)), \tag{A.4}$$

where

$$\begin{aligned} \tilde{\omega}_j &= \frac{p_{j+1}-p_{j-1}}{p_{j+2}-p_{j-2}}; \\ \kappa_j &= \max\left(0, \frac{\tilde{\kappa}_j - \kappa^{(1)}}{\tilde{\kappa}_j + \kappa^{(2)}}\right), \end{aligned} \tag{A.5}$$

where

$$\tilde{\kappa}_j = \frac{W_j + C_{j-2s_j}}{W_j}$$

and

$$W_j = \left(\frac{\max(p_{j+2}, p_{j-2}) + \frac{1}{2}(\gamma-1)(p_{j+2}+p_{j-2})}{\max(\tau_{j+2}, \tau_{j-2})}\right)^{1/2}.$$

Here, W_j is an estimate of the Lagrangian shock speed, and C_{j-2s_j} the post-shock wave speed. The quantity $\tilde{\kappa}_j$ is the number of equally spaced zones that a signal can travel from a shock in the length of time that it takes a shock to cross one such zone; in the limit of very small time steps it is a measure of the wavelength of the

fundamental mode of any potential noise behind the shock. The flattening coefficient is then defined to be

$$f_i = \max(\tilde{f}_{j-1}, \tilde{f}_j, \tilde{f}_{j+1}), \tag{A.6}$$

where

$$\tilde{f}_j = \min(w_j \omega_j, \kappa_j).$$

Thus we are using the smaller of the two amounts of flattening given by the wavelength and steepness criteria. In the calculations shown above, $\kappa^{(1)} = 2$, $\kappa^{(2)} = 0.01\omega^{(1)} = 0.75$, $\omega^{(2)} = 10$. The flattening provides enough dissipation so that the Lagrangian scheme produces acceptably oscillation-free steady shock profiles. However, it is necessary to introduce a small amount of dissipation such as in (4.2) or (4.3) if one wishes to eliminate some types of starting errors, such as those occurring for shock tube initial data.

For multidimensional Eulerian calculations, we use a combination of flattening and local mesh motion (4.3) to introduce the required dissipation. For the flattening, we have the parameters κ_j and ω_j, which, as before, depend on the wavelength of the noise and the steepness of the shock profile. We also introduce a third parameter, σ_j, which depends on the strength of the wave:

$$\sigma_j = \max\left(0, \frac{\tilde{\sigma}_j - \sigma^{(1)}}{\tilde{\sigma}_j + \sigma^{(2)}}\right), \tag{A.7}$$

where

$$\tilde{\sigma}_j = w_j \frac{|p_{j+2} - p_{j-2}|}{\min(p_{j+2}, p_{j-2})};$$

$$\omega_j = \max(0, \omega^{(1)}(\omega^{(2)} - \tilde{\omega}_j)), \tag{A.8}$$

where

$$\tilde{\omega}_j = \max\left(\frac{p_{j+1} - p_{j-1}}{p_{j+2} - p_{j-2}}, \frac{E_{j+1} - E_{j-1}}{E_{j+2} - E_{j-2}}\right);$$

$$\kappa_j = \max\left(0, \frac{\tilde{\kappa}_j - \kappa^{(1)}}{\tilde{\kappa}_j + \kappa^{(2)}}\right), \tag{A.9}$$

where

$$\tilde{\kappa}_j = \left|\frac{W_j^E - u_{j+2s_j} + s_j c_{j+2} s_j}{W_j^E}\right|$$

and

$$W_j^E = s_j \frac{W_j}{\rho_{j-2} s_j} + u_{j-2} s_j,$$

with

$$W_j = \left(\frac{\max(p_{j+2}, p_{j-2}) + \frac{1}{2}(\gamma - 1)(p_{j+2} + p_{j-2})}{\max(\tau_{j+2}, \tau_{j-2})}\right)^{1/2}.$$

The flattening coefficient is then defined to be

$$f_i = \max(\tilde{f}_j, \tilde{f}_j + s_j), \tag{A.10}$$

where

$$\tilde{f}_j = \min(w_j \omega_j, w_j \sigma_j, \kappa_j).$$

We also use the parameters defined above in constructing our grid velocity v_j:

$$\tilde{v}_{j+1/2} = \nu^{(1)} \max(-(D \cdot \vec{u})_{j+1/2,k}, 0), \tag{A.11}$$

where

$$(D \cdot \vec{u})_{j+1/2,k} = u_{j+2} - u_{j-1} + ((v_{j+1,k+2} + v_{j,k+2}) - (v_{j+1,k-2} + v_{j,k-2})) \times \frac{r_{j+2} - r_{j-1}}{2(z_{k+2} - z_{k-2})},$$

and

$$v_{j+1/2} = s_{j+1/2} \min\left(\max(\tilde{v}_{j-1/2}, \tilde{v}_{j+1/2}, \tilde{v}_{j+3/2}), (\nu^{(2)} + \nu^{(3)} \max(\sigma_j \kappa_j^2, \sigma_{j+1} \kappa_{j+1}^2)) \times \frac{\Delta r_{j+2} s_{j+1/2}}{\Delta t}\right).$$

When using this dissipation with the two-step Eulerian method, the flattening is applied at the beginning of the Lagrangian step; no flattening is applied to the interpolations performed for the remap. Obviously, the local grid motion only affects the remap step, in determining the grid which one maps back to. The constants which were used in this form of dissipation for the calculations in [2] were $\nu^{(1)} = 2$, $\nu^{(2)} = 0.1$, $\nu^{(3)} = 0.2333$, $\omega^{(1)} = 0.75$, $\omega^{(2)} = 10$, $\kappa^{(1)} = 2$, $\kappa^{(2)} = 0.01$, $\sigma^{(1)} = 0.5$, $\sigma^{(2)} = 1$. For one-dimensional calculations, we set $\nu^{(2)} = 0$ and $\nu^{(3)} = 0.3333$. Fairly exhaustive test calculations of steady shock structures covering the whole parameter space for a polytropic gas with $\gamma = 1.4$ gave rise to this choice of parameters. The amplitude of oscillations in the post-shock density was $\frac{2}{3}$% of the density jump in the worst case, and is more typically $\frac{1}{4}$%. The oscillations in other variables were much

smaller. For all but nearly stationary shocks, any such oscillations are rapidly damped downstream from the shock. The effective shock width is never more than two mesh lengths, and for rapidly moving shocks it is one mesh length. Experimentation with different values of the parameters is not recommended, as these choices have been made on the basis of considerable experience.

Acknowledgments

This work was performed under the auspices of the Director, Office of Energy Research, Office of Basic Energy Sciences, Engineering, Mathematical, and Geosciences Division of the U.S. Department of Energy at the Lawrence Berkeley Laboratory under Contract DE-AC03-76SF00098, and at the Lawrence Livermore National Laboratory under Contract W-7405-ENG-48.

References

1. P. R. Woodward and P. Colella, *Lecture Notes in Physics* **141** (1981), 434.
2. P. R. Woodward and P. Colella, *J. Comput. Phys.* **54** (1984), 115–173.
3. S. K. Godunov, *Mat. Sb.* **47** (1959), 271.
4. S. K. Godunov, A. V. Zabrodin, and G. P. Prokopov, *U.S.S.R. Computational Math. and Math. Phys.* **1** (1961), 1187.
5. B. van Leer, *J. Comput. Phys.* **32** (1979), 101.
6. B. van Leer and P. R. Woodward, Proceedings TICOM Conference, Austin, Texas, 1979.
7. P. Colella, A direct Eulerian MUSCL scheme for gas dynamics, *SIAM J. Sci. Statist. Comput.*, in press.
8. B. van Leer, *J. Comput. Phys.* **23** (1977), 276.
9. B. van Leer, private communication.
10. R. Courant and K. O. Friedrichs, "Supersonic Flow and Shock Waves," Wiley–Interscience, New York, 1948.
11. A. Lapidus, *J. Comput. Phys.* **2** (1967), 154.
12. P. Colella and H. M. Glaz, Efficient solution algorithms for the Riemann problem for real gases, in preparation.

Printed by the St. Catherine Press Ltd., Tempelhof 41, Bruges, Belgium